Impact of the Unstirred Water Layer on the Permeation of Small-Molecule Drugs

Christopher Kang, Alyson Shoji, Christophe Chipot, Rui Sun

The Impact of the Unstirred Water Layer on the Permeation of Small Molecule Drugs

Christopher Kang,[†] Alyson Shoji,[‡] Christophe Chipot,[¶,§,‖] and Rui Sun[*,†]

†*Department of Chemistry, The University of Hawai'i at Manoa, Honolulu, HI 96822, USA*

‡*Department of Chemistry, University of Washington, Seattle, WA 98105, USA*

¶*Laboratoire International Associé Centre National de la Recherche Scientifique et University of Illinois at Urbana-Champaign, Unité Mixte de Recherche n°7019, Université de Lorraine, B.P. 70239, 54506, Vandœuvre-lès-Nancy cedex, France*

§*Theoretical and Computational Biophysics Group, Beckman Institute, and Department of Physics, University of Illinois at Urbana-Champaign, Urbana, IL 61801, USA*

‖*Department of Biochemistry and Molecular Biology, University of Chicago, Chicago, IL 60637, USA*

E-mail: ruisun@hawaii.edu

Abstract

Over the last two decades, numerous molecular dynamics (MD) simulation-based investigations have attempted to predict the membrane permeability to small-molecule drugs as indicators of their bioavailability, a majority of which utilize the inhomogeneous solubility diffusion (ISD) model. However, MD-based membrane permeability is routinely 3 to 4 orders of magnitude larger than the values measured with intestinal perfusion technique. There have been contentious discussions on the sources of the large discrepancies, and the two indisputable, potentially dominant ones are the fixed protonation state of the permeant and the neglect of the unstirred water layer (UWL). Employing six small-molecule drugs of different biopharmaceutical classification system (BCS) classes, the current MD study relies on the ISD model, but introduces the (de-)protonation of the permeant by characterizing the permeation free energy of both neutral and charged states. In addition, the role of the UWL as a potential resistance against permeation is explored. The new MD protocol closely mimics the nature of small-molecule permeation, and yields estimates that agree well with *in vivo* intestinal permeability.

Introduction

Oral administration remains the overwhelmingly favored route of drug delivery due to numerous advantages such as safety, cost, and patient compliance.[1] One of the outstanding challenges in the discovery process of orally administered drugs is the *a priori* knowledge of pharmacokinetics, in particular, the rate of intestinal permeation, which critically influences the absorption and distribution of a drug.[2–4] Although the intestinal permeability measured by the intestinal perfusion technique ($P_{\text{eff}}^{\text{int}}$) is often considered the gold standard due to its remarkable correlation with the bioavailability (i.e., the percentage of the drug-like molecule that enters systemic circulation),[5,6] the experiment itself is invasive, expensive, and laborious. As a result, there are only limited data available compared to permeabilities measured from *in vitro* assays (P_{app}), e.g., utilizing compartmentalized solutions of permeants of different concentrations separated by an artificial cell monolayer, where P_{app} corresponds to the ratio of the net flux of permeant across the monolayer. Depending on the conditions of the *in vitro* assays as well as the experimental apparatus, P_{app} is often subject to substantial (typically spanning an order of magnitude) variations between studies.[7–9] Accompanying these experimental assays, computational methods, namely quantitative structure–property relationship (QSPR) approaches, have been used to predict permeabilities.[10,11] Yet, their strengths lie in existing experimental determinants and could therefore be of limited practical use for predicting properties of novel drug candidates.

The total resistance to intestinal permeation of small molecule drugs arises from a series of barriers such as the membrane, unstirred water layer (UWL) and chemical environment,[12] among others, which can be viewed as a sum of resistors in series:

$$\frac{1}{P_{\text{eff}}} = \frac{1}{P_{\text{m}}} + \frac{1}{P_{\text{UWL}}} + \frac{1}{P_{\text{c}}} + ... = R_{\text{eff}} = R_{\text{m}} + R_{\text{UWL}} + R_{\text{c}} + ... \tag{1}$$

Where P_{eff} is the apparent intestinal permeability; R_{m} is the intrinsic membrane resistance, resulting in the time lag between a permeant submerging into one leaflet and emerging from

the opposing leaflet; R_{UWL} is the resistance of the unstirred water layer (UWL), resulting in the time lag between a permeant reaching the surface of the membrane from the bulk of the gastrointestinal fluid; R_{c} is the resistance of the chemical environment, resulting in the time lag for a permeant to switch its protonation state (e.g., the ionic form of the permeant (de-)protonates to its neutral form before entering into hydrophobic core of the membrane).

As numerous advances on the hardware and algorithmic, as well as in the underlying theory have been made,[13–16] molecular dynamics (MD) simulation-based studies have shown promises of being an efficient and cost-effective alternative to measuring permeability experimentally.[17–20] Although alternatives are gaining steam,[21–23] an overwhelming majority of MD-based permeation studies rely on the inhomogeneous solubility diffusion (ISD) model.[17–20,24,25] The ISD model is built upon the homogeneous solubility diffusion model,[26,27] i.e., the permeability of cells to different permeants is proportional to their octanol-water partition coefficient, K. Assuming a quasi-steady distribution of a solute on both sides of the cell, Fick's Second Law states that:

$$P = KD/h \tag{2}$$

where D is the diffusivity of the permeant through the membrane and h is the thickness of the latter. This model assumes that the partitioning and diffusion of the permeants are uniform throughout the membrane. However, membranes are made of lipid molecules consisting of hydrophilic head groups and hydrophobic tail groups, so that their interaction with permeants varies along the transmembrane axis (conventionally, the z-direction of Cartesian space). To address this oversimplification, in 1974, Diamond and Katz[28] proposed the ISD model:

$$\frac{1}{P} = \int_{-0.5}^{+0.5} \frac{1}{K(\xi)D(\xi)}\,\mathrm{d}\xi \tag{3}$$

according to which the partition coefficient K and diffusivity D depend on the position, ξ of the permeant as it traverses the membrane. We note ξ is the reduced permeation coordinate, which expands from the bulk solution -6.5 nm outside one leaflet (-0.5) to the bulk solution

+6.5 nm outside the opposing leaflet (+0.5). Assuming the permeation is a near equilibrium process, $K(\xi)$ can be related to the free energy of the permeation, $G(\xi)$, as:

$$K(\xi) = \frac{1}{\exp[\beta G(\xi)]} \tag{4}$$

in which $\beta = 1/k_B T$. Thus equation 3 can be rewritten as:

$$R_{\mathrm{m}} = \frac{1}{P_{\mathrm{m}}} = \int_{-0.5}^{+0.5} \frac{\exp[\beta G(\xi)]}{D(\xi)}\, \mathrm{d}\xi \tag{5}$$

$G(\xi)$ can be accessed *via* MD simulations enhanced with importance-sampling methods, and $D(\xi)$ can be evaluated in MD simulations by force or position auto-correlation function calculation, or Bayesian inference.[17,29] We emphasize that the subscript "m" is added to the equation as the resistance R only takes into account the membrane instead of other factors listed in Eq. 1. It should not be a surprise that in spite of employing a diverse pool of methodologies for computing $G(\xi)$ and $D(\xi)$, MD simulations repeatedly demonstrate that P_{m} predicted by the ISD model[5,17,19,30] is routinely 3 to 4 orders of magnitude larger than the intestinal perfusion permeability $P_{\mathrm{eff}}^{\mathrm{int}}$. Although numerous factors could contribute to inaccuracies in P_{m}, including uncertainties associated with the force fields,[31] the imperfect convergence of the free energy calculation, $G(\xi)$,[18,20,32] the ambiguous nature of permeant diffusion inside the membrane (i.e., diffusion vs. subdiffusion),[17] as well as the oversimplified lipid bilayer employed in the simulation,[18,33,34] the impact of these issues has either been well investigated or can be mitigated[17,30]. In other words, these issues alone are not primarily responsible for the observed large discrepancies between P_{m} and $P_{\mathrm{eff}}^{\mathrm{int}}$. Recall Eq. 5, and as noted previously, the resistance determined here, R_{m}, is indeed only one component of the effective resistance (R_{eff}, Eq. 1) and indicates P_{m} is a reasonable approximation of P_{eff} only if R_{m} overwhelms all other resistances. Therefore, P_{m} is not necessarily the dominating factor in controlling the permeation of small molecules.

The UWL adjacent to the intestinal membrane has long been regarded as a barrier for

intestinal absorption of compounds.[12,35,36] As demonstrated by Avdeef et al.,[37] stirring (thus decreasing the thickness of UWL) can increase the permeability by up to a few orders of magnitude for a series of small molecule drugs. Although the exact thickness of the UWL in the GI tract varies between experiments, most of the reported thickness ranges between 30 and 100 μm.[6,27,38–40] As noted in a recent review,[30] all MD-based permeation studies use water layers of only a few nm above and below the membrane. Therefore, although P_{m} obtained in such simulations technically includes both P_{m} and P_{UWL}, the impact of the latter is grossly underestimated.[41] To our best knowledge, due to the spacial limitation of conventional MD simulations, there has not been an MD-based study fully characterizing the impact of the UWL as a potential resistor to permeation. However, experimentally, it has been shown that in the case of fast permeants (e.g., ketoprofen, propranolol), the resistance to permeation as result of the UWL (R_{UWL}) completely overshadows the intrinsic membrane resistance,[42] i.e., R_{m}.

Passive permeation of charged molecules is expected to be forbidden due to the associated high free energy barrier of an ionized species entering a hydrophobic medium. Therefore, almost all of the MD-based studies have focused exclusively on the permeation of the neutral form of the molecule. Still, under physiological conditions of gastrointestinal fluids, most of the small molecules are charged—take ketoprofen ($\mathrm{p}K_{\mathrm{a}} = 4.0$) as an example, only about 0.1–1% are in the neutral form in the gastrointestinal fluid with a pH of approximately 6.5–7.5.[43,44] It is important to note that in principle, the ISD model does not limit the free energy of permeation ($G(\xi)$ in Eq. 5) to a single protonation state and there have been pioneering investigations (e.g., Zhi et al.[45]) on the impact of (de-)protonation of the permeant with constant-pH MD simulations. However, this method is more expensive than conventional MD simulations, hampering its application to a series of small-molecule drugs in general.

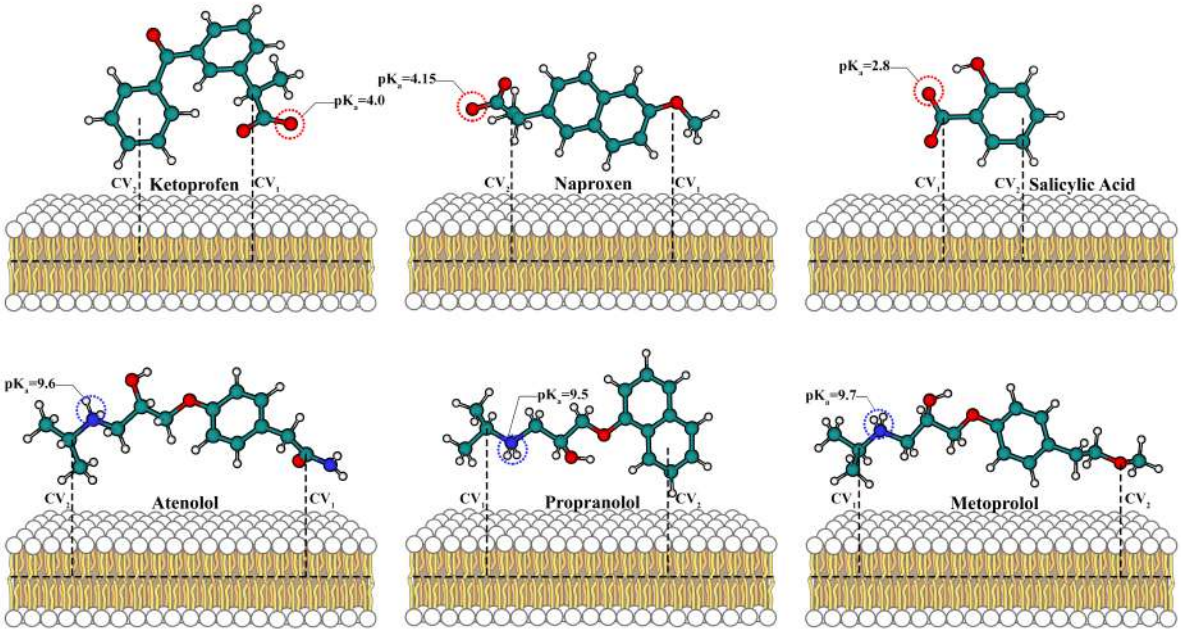

Figure 1: Illustrations of the structures, pK_{a}, collective variables, and protonation/deprotonation groups (dashed circle) for the small molecule drugs in this study. The distances between each of the terminal ends to the center of mass of the lipid bilayer are employed as collective variables.

In this manuscript, we investigate the permeation of six different small molecules (ketoprofen, metoprolol, atenolol, naproxen, propranolol, and salicylic acid) with MD simulations (Figure 1). The new protocol reported in this manuscript accounts for the impact of the UWL, which varies according to the identity of the permeant. In addition, the (de-)protonation is also accounted for by characterizing the permeation free energy at different protonation states of the permeant. Our results show good agreement with the permeabilities measured using the intestinal perfusion technique, and reveal that traversing the UWL, instead of the lipid bilayer, is the rate-limiting step for fast permeants (e.g., ketoprofen, naproxen or propranolol).

Results

The Free Energy of Permeation, $G(\xi)$

All small-molecule drugs studied in this manuscript (Fig.1) possess only one protonatable group and their pK_a values deviate from 7.0 by at least 2.5 log units. Therefore, the overwhelming majority of them should be in the ionic form when diffusing in the GI tract. Take the permeation of ketoprofen (pK_a = 4.0) as an example again, where in a pH 7 solution, its anionic form make up 99%+ of the population.[46]

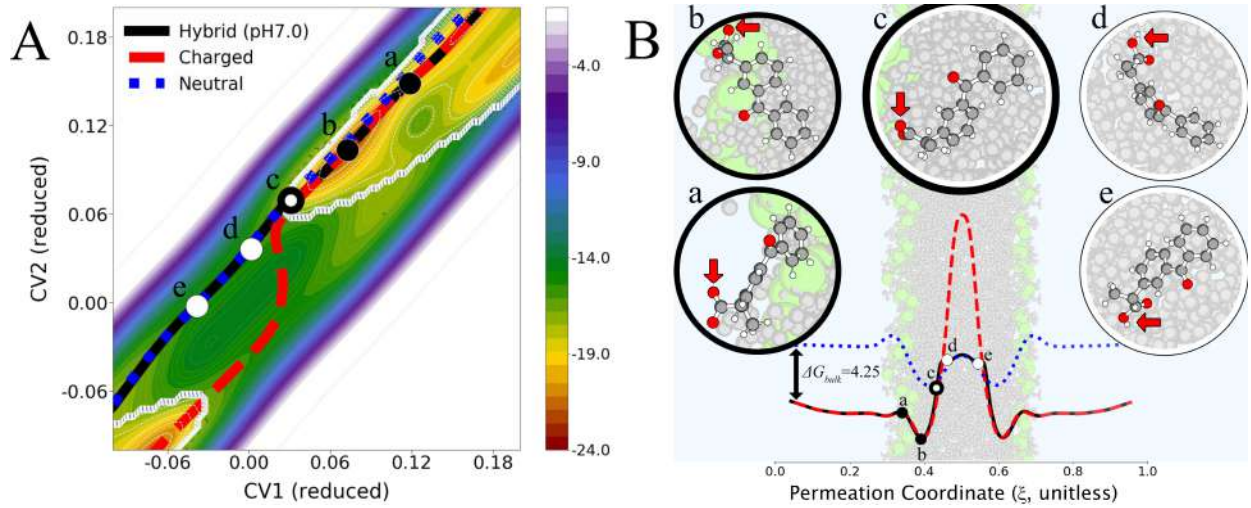

Figure 2: (A) Hybrid free energy surface for the permeation of ketoprofen. It is made from overlaying the surface of the charged permeant (enclosed by white lines) and the surface of the neutral permeant. Black (point a and b) and white (point d and e) circles indicate configurations on the charged and neutral surface, respectively. Point c corresponds to a configuration where the (de-)protonation takes place. (B) Neutral, charged and hybrid MFEPs of ketoprofen ketoprofen, showing the separation (ΔG_{bulk}) between the neutral and charged ketoprofen in bulk. Points a to e are synchronized across both panels, indicating ketoprofen traversing the membrane with the protonatable group highlighted by a red arrow.

The minimal free energy path (MFEP) of the permeation, calculated with the zero-temperature string method,[47] suggests that the membrane presents a major permeation barrier (+17 kcal/mol, see Fig.2.B) to the anionic form of ketoprofen. In contrast, the lipid bilayer acts as a shallow well (−4 kcal/mol, see Fig.2.B) to its neutral form. For all the small-molecule drugs studied, including both acids and bases, the membrane presents a 15-20 kcal/mol bar-

rier to permeation of charged species (Fig. 3). This result, consistent with our understanding that charged molecules do not traverse the membrane *via* passive permeation, suggests that the net charge overwhelms the chemical properties of the small-molecule drug (e.g., acid *vs.* base; hydrophobic *vs.* hydrophilic). The neutral form of all small-molecule drugs possess a much smaller permeation barrier (-3 to +5 kcal/mol) compared to their charged counterpart (Fig. 3). It is indicative that the lipid bilayer is a permeation barrier for hydrophilic molecules (e.g., atenolol) and a free energy well for lipophilic molecules (e.g., ketoprofen). A more detailed discussion on the permeation mechanism of neutral small-molecule drugs can be found in Ref. 19.

The p$K_{\rm a}$ value corresponds to the free energy difference between the charged form and the neutral form of the small molecule drugs in gastrointestinal fluid (assume pH 7).

$$\Delta G_{\rm bulk} = -2.3 k_B T ({\rm p}K_{\rm a} - {\rm pH}) \tag{6}$$

$\Delta G_{\rm bulk}$, the ionization free energy, gives the basis for overlaying the free energy surfaces of permeation of the same molecule in two different protonation states, i.e., the free energy of the permeation of the neutral form is shifted up by $\Delta G_{\rm bulk}$. The overlaying of the free energy surfaces (Fig.2.A and Fig. S1 in the Supporting Information) result in seams that correspond to the position where the charged and neutral forms of the molecule have the same free energy. Their respective population should be equal under the assumption of chemical equilibrium. In such a case, the true free energy of permeation is the hybrid surface of the two, where the small molecule drug always resides on the lower free energy surface. The hybrid permeation MFEP, that allows the permeant to be in different protonation states is obtained from the hybrid surface. As shown in Fig. 3, the hybrid MFEP significantly reduces the effective barrier against permeation compared to the ionic form, and slightly increases it compared to the neutral form.

It is important to verify the assumption (i.e., the charged and neutral form of the small

molecule drugs can interchange from one form to another) that leads to the hybrid permeation MFEP. The (de-)protonation of these small-molecule drugs can take place only when there is access to water molecules, e.g., in bulk water, or near the head-group region where lipid packing defects allow solvent access.[48,49] Fig. 2 shows snapshots of a representative configuration where ketoprofen is at different positions along the hybrid MFEP with respect to the lipid bilayer. As illustrated, ketoprofen is in the anionic form approaching the lipid bilayer (point a). At the interface (from point b and c), the hydrophobic moiety of ketoprofen inserts into the acyl-chain region of the lipids, while leaving the carboxylate group in the head group region. Further insertion (from point c and d) requires the carboxylate group (anion) to gain a proton and transform into the carboxyl group (neutral). Note these actions take place *via* transiting from the charged free energy surface to the neutral free energy surface at the seam. The inserted configuration of point c reveals that the carboxylate group is right beneath the head group regions of the lipid bilayer; thus, it should have access to water molecules to let protonation occur. Ketoprofen remains in its neutral form as it traverses the lipid tails (points d to e) to reach the opposing leaflet. We note that the permeation free energy surfaces of neutral and charged species, as well as the hybrid surfaces of all permeants studied here can be found in Fig. S2, S3 and S4, respectively. Their (de-)protonation configurations are verified to be near the lipid head group region (Fig.S5), and, hence, have access to water molecules.

The Effective Permeability from MD Simulations, $P_{\mathrm{eff}}^{\mathrm{MD}}$

As Eq. 5 indicates, the position-dependant diffusion coefficients $D(\xi)$ is required to compute the permeability. $D(\xi)$ for the six small molecule drugs are computed following the protocol described in the Method section, and shown in the Figure S6. The diffusion coefficient profile of the neutral species agrees with previous studies[19,25] (i.e., on the order of 10^{-5} cm^2/s in bulk and 10^{-6} cm^2/s in the acyl-chain). Compared to their neutral counterpart, the diffusion coefficients of the charged species on average are nearly halved in the bulk

Table 1: Physicochemical properties and computed intrinsic permeability of six small molecule drugs. $\delta_{\mathbf{UWL}}$ is the effective thickness of the UWL. $\boldsymbol{P}_{\mathbf{eff}}^{\mathbf{int}}$ is the permeability measured with the intestinal perfusion technique by Dahlgren et al.[5] $\boldsymbol{P}_{\mathbf{m}}$ is the permeability calculated by the ISD model and $\boldsymbol{P}_{\mathbf{m}}^{*}$ is permeability calculated by the hybrid, protonable model. $\boldsymbol{P}_{\mathbf{UWL}}$ is the permeability of the UWL. $\boldsymbol{P}_{\mathbf{eff}}^{\mathbf{MD}}$ is the effective permeability, calculated with contributions from $\boldsymbol{P}_{\mathbf{m}}^{*}$ and $\boldsymbol{P}_{\mathbf{UWL}}$ (Eq.1).

Drug	pK_{a}	δ_{UWL}	log$P_{\mathrm{eff}}^{\mathrm{int}}$	logP_{m}	logP_{m}^{*}	logP_{UWL}	log$P_{\mathrm{eff}}^{\mathrm{MD}}$
Ketoprofen	4.0	35.8	-3.06	0.15	-1.42	-3.80	-3.80
Metoprolol	9.7	31.1	-3.87	-0.12	-0.76	-3.92	-3.92
Naproxen	4.2	38.4	-3.07	-0.03	-0.73	-3.73	-3.74
Propranolol	9.5	53.0	-3.54	0.21	0.38	-3.46	-3.45
Salicylic Acid	2.8	58.6	-3.72*	0.05	-4.19	-3.37	-4.25
Atenolol	9.6	40.6	-4.70	-1.86	-4.58	-3.69	-4.63

* Interpolated value based on intestinal permeability of the other 5 small-molecule drugs (see Fig.S7)

aqueous region. The diffusion coefficients of neutral and charged species are comparable within the hydrophobic core of the lipid bilayer. Two types of ISD-predicted permeabilities (Eq.5) are reported in Table 1—one corresponds to the permeation of neutral species P_{m}, and the other corresponds to the aforementioned hybrid species that allows (de-)protonation, P_{m}^{*}. To compute P_{m}^{*}, the diffusion coefficient of the permeant, $D(\xi)$, is obtained from the corresponding protonation states. In accordance with other MD studies,[18,25,50,51] the ISD model for neutral species (P_{m}) significantly overestimates the permeability by three to four orders of magnitude compared to $P_{\mathrm{eff}}^{\mathrm{int}}$ obtained from intestinal perfusion assays. Although more closely mimicking the permeation process, the result of $\mathrm{P}_{\mathrm{m}}^{*}$ suggests that allowing (de-)protonation to occur does not fix the overestimation observed with the ISD model, except for the case of atenolol and salicylic acid, the MD-predicted permeability of which is very close to $P_{\mathrm{eff}}^{\mathrm{int}}$. It is noteworthy that these two drugs are also the two most hydrophilic among the six (see Fig.1) and possess higher hybrid permeation free energy barriers (see Fig.3C). It should be reminded here that according to the ISD model, the permeability scales linearly with the diffusion coefficient, but exponentially with the free energy (Eq. 5). Small differences in the diffusion coefficient are, therefore, unlikely to address the nearly three-order of magnitude

difference in P_{m} and P_{m}^{*}.[17]

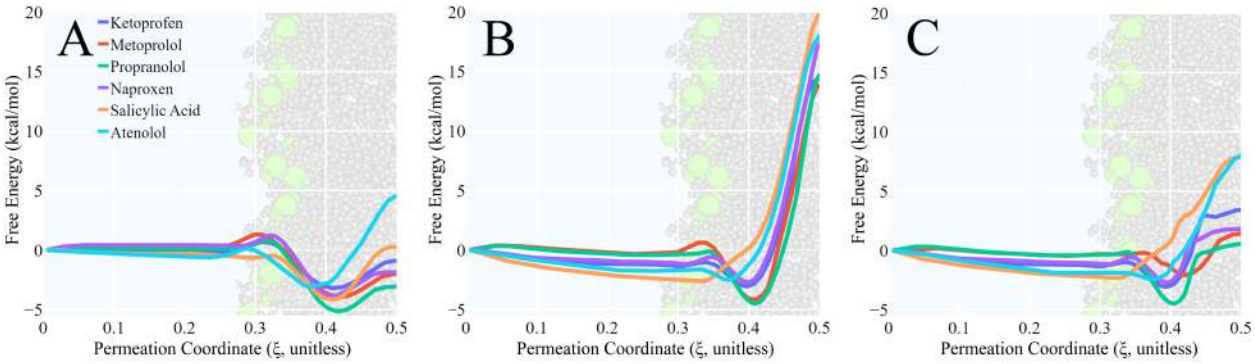

Figure 3: MFEPs of the permeation of the neutral (A) and charged (B) small molecule drugs. The hybrid MFEPs (C) that allow for the (de-)protonation during the permeation.

The Rate-limiting Step of Small-Molecule Drug Permeation

P_{m} and P_{m}^{*} predicted from the ISD model only accounts for the membrane as the sole resistance against permeation. The UWL is a stagnant layer of water adjacent to the lipid bilayer on the epithelial side of the intestine. The UWL is not subject to the convective mixing of the bulk solution (e.g., as a result of peristalsis),[52,53] and the diffusion through it could act as an additional barrier against absorption of small molecules. It has been reported since the early 70s that the UWL could act as a significant resistance against permeation of small molecule drugs. For example, Avdeef et al.[37] showed a two-to-three-order of magnitude increase in *in vitro* permeability if the solution is stirred (i.e., decreasing the thickness of the UWL). The set of molecules used by Avdeef et al. includes several molecules utilized in our study (e.g., propranolol, metoprolol, and atenolol). As noted in the previous section, the thickness of the UWL is grossly underestimated in all MD simulations, as the thickness of the water compartments is only a few nm, in contrast to 30-100 μm under physiological condition.[6,27,38–40] To compare the MD-based permeability $P_{\mathrm{eff}}^{\mathrm{MD}}$ with the intestinal perfusion permeability $P_{\mathrm{eff}}^{\mathrm{int}}$ (see Table.1), it is important to develop a model to account for the resistance introduced by the UWL. This term, R_{UWL} is estimated from the

diffusion coefficient (D) and the thickness of the UWL (δ_{UWL}):

$$R_{\mathrm{UWL}} = \frac{1}{P_{\mathrm{UWL}}} = \frac{\delta_{\mathrm{UWL}}}{D} \tag{7}$$

Although the exact thickness of UWL in the GI-tract is still up for debate, it has been reported[53] that δ_{UWL} is molecule-dependant, e.g., small molecules with a larger diffusion coefficient encounter an apparently thicker UWL than larger molecules with a smaller diffusion coefficient. Qualitatively, it has been shown that δ_{UWL} of two different molecules (subscript 1 and 2 in the following equation) can be related to their diffusion coefficient in bulk water as:

$$\frac{\delta_{\mathrm{UWL},1}}{\delta_{\mathrm{UWL},2}} = \left(\frac{D_1}{D_2}\right)^{1/3} \tag{8}$$

In this research, δ_{UWL} for each of the small molecule is calibrated with glucose (8), the UWL thickness[39] of which (40 μm) and diffusion coefficient[40] ($8.0 \times 10^{-6}\mathrm{cm}^2/\mathrm{s}$) have been established from measurements in the human small intestine. We note that this thickness is on the lower side of the commonly-accepted range of UWL thicknesses (30-100 μm of small-molecule drugs) and, therefore, should offer a conservative estimate of the UWL resistance. The results are summarized in Table 1. The permeability values associated with the UWL alone (P_{UWL} from Eq. 1) are also gathered in Table 1.

Finally, the effective permeability from MD simulations ($P_{\mathrm{eff}}^{\mathrm{MD}}$, Eq. 1) is computed based on both the intrinsic permeability (P_{m}^{*}) and the UWL permeability (P_{UWL}). As noted in the previous section, although P_{m}^{*} accounts for the potential (de-)protonation of the permeants as they traverses the membrane, it is important to emphasize that the titration of the drug molecules is not an instantaneous event. In actuality, the resistance associated with the chemical environment (R_{c}, Eq. 1) results in (de-)protonation kinetics that span timescales similar to those of membrane permeation.[54] Nonetheless, $P_{\mathrm{eff}}^{\mathrm{MD}}$should provide the most commensurable comparison with $P_{\mathrm{eff}}^{\mathrm{int}}$ measured by means of the intestinal perfusion technique. As shown in Table 1, $P_{\mathrm{eff}}^{\mathrm{MD}}$agrees remarkably well with $P_{\mathrm{eff}}^{\mathrm{int}}$ for the six permeants of this

study. The minimum, maximum, and mean absolute deviation are only 0.05 (metoprolol), 0.74 (ketoprofen), and 0.35 log units, respectively. This agreement is very good compared to previuous state-of-the-art ISD studies (where the role of protonation/deprotonation and diffuson through the UWL is neglected), yielding estimates typically off by a few log units. Given the fact that there are still other potential sources of statistical and systematic errors (e.g., force-field inaccuracies, and suboptimal convergence) as mentioned in the introduction, this result suggests that the proposed model, i.e., a combination of the hybrid permeation free energy that allows for the (de-)protonation of the permeant and the resistance arising from the diffusion through the UWL captures the nature of permeation of small-molecule drugs very well.

Table 1 also paints a potentially grim picture of the MD-based approach to estimating the membrane permeability to small-molecule drugs as it suggests that the rate-limiting step of the intestinal permeation is not necessarily associated with the permeant traversing the membrane (i.e., P_{m}^{*}). For all the permeants of this study but atenolol and salicylic acid, the resistance associated with the diffusion through the UWL overwhelmingly contributes to the resistance against permeation, e.g., the permeability associated with UWL, P_{UWL}, is within 0.05 log unit from the simulation predicted permeability ($P_{\mathrm{eff}}^{\mathrm{MD}}$) and has a mean absolute deviation of only 0.30 log units from the experimental intestinal permeability ($P_{\mathrm{eff}}^{\mathrm{int}}$). In other words, for ketoprofen, metoprolol, naproxen, and propranolol diffusing through the UWL, as opposed to permeating through the membrane, is the rate-limiting step. This result is in agreement with Avdeef et al.'s series of permeability measurements with in vitro assays,[37,55] where a strong correlation between the stirring rate and permeability was reported. Therefore, although MD simulations aimed at assessing the intrinsic membrane permeability (P_{m}^{*}) consume the overwhelming majority of the computer time (over 98% in this study), the bulk of this computational effort can have a negligible effect on the $\mathrm{P}_{\mathrm{eff}}^{\mathrm{MD}}$for some, if not the vast majority of small-molecule drugs.

For atenolol and salicylic acid, traversing the membrane is, indeed, the rate-limiting

step. As indicated in Table 1, the resistance of the UWL only accounts for 11% and 13% of the total resistance agianst permeation, respectively. For these permeants, extensive MD simulations appear justified to assess P_{m}^{*} with adequate accuracy. These results, therefore, beg the question as to how one distinguishes membrane-permeation-limited molecules from UWL-diffusion-limited molecules. The ISD model suggests (Eq. 5) that those molecules characterized by a high permeation free energy barrier also correspond to a slow permeation across the membrane, more likely making it the rate-limiting step. As shown in Fig. 3.C, atenolol and salicylic acid have significantly higher free-energy barriers against permeation than other permeants—they are the ones demonstrating the most membrane-permeation-limited behavior. In addition, it is also important to note that in order to obtain an accurate account of P_{m}^{*}, the permeation free energy should be obtained from the *hybrid* MFEP, which mirrors the (de-)protonation of the permeants as they translocate across the membrane, instead of keeping them in a neutral form. All other small-molecule drugs have a small enough barrier that the effective permeability, $P_{\mathrm{eff}}^{\mathrm{MD}}$, is completely dominated by the diffusion through the UWL, P_{UWL}.

To efficiently obtain MD-based permeability ($P_{\mathrm{eff}}^{\mathrm{MD}}$) that agrees well with the intestinal perfusion permeability $P_{\mathrm{eff}}^{\mathrm{int}}$, a guiding principle should, therefore, be established based on the *hybrid* free energy barrier—if it is less than a certain threshold, then the focus should be on computing the effective thickness of the UWL and diffusion coefficient, instead of the long, laborious free-energy calculation of membrane permeation. To assess this threshold, we put forth a hypothetical molecule of permeation free energy, $G_x(\xi)$, expressed as an ad-hoc combination of the permeation free energy of atenolol (membrane-limited, hybrid $G_a(\xi)$ in Fig.3.C) and ketoprofen (diffusion-limited, hybrid $G_k(\xi)$ in Fig.3.C):

$$G_x(\xi) = c_a G_a(\xi) + c_k G_k(\xi) \tag{9}$$

where c_a and c_k are the weight associated with $G_a(\xi)$ and $G_k(\xi)$, respectively, and $c_a + c_k =$

1. By varying c_a and c_k, it turns out that the intrinsic membrane permeability, P_{m}^{*}, will contribute more than 10% of $P_{\mathrm{eff}}^{\mathrm{MD}}$if the height of the barrier is more than 5.6 kcal/mol (maximum of $G_x(\xi)$). This number is calculated assuming that the diffusion coefficient of the hypothetical molecule is also a linear combination of the diffusion coefficient of atenolol and ketoprofen with the same weights (i.e., $D_x(\xi) = c_a D_a(\xi) + c_k D_k(\xi)$). In other words, for the purpose of faster screening, one only needs to focus on the diffusion through the UWL if the height of the permeation barrier is less than 5.6 kcal/mol. However, it is important to realize that the hybrid free energy barrier is *not* the readily-available partitioning coefficient between the aqueous and the oil phase. As shown in Fig.3, although arguments can be made based on the hydrophobicity of the permeant, assessing its hybrid free energy barrier accurately is not trivial (e.g., atenolol vs. salicylic acid) and requires appropriate free-energy calculations. However, one can still expect that as more computational studies are conducted, a database of hybrid free energy barriers could be built for small-molecule drugs and one can make a reasonable inference as to whether the major resistance against permeation for a new, chemically analogous permeant stems from membrane crossing or diffusion through the UWL.

Discussion and Conclusions

Applications of the Model

Studying the permeability of small molecule drugs with the ISD model on their neutral form (P_{m}) overestimates the permeability ($P_{\mathrm{eff}}^{\mathrm{MD}}$, see Table 1) by 3-4 orders of magnitude, P_{m} has been reported as an indicator of the *relative* permeability (i.e., rank the permeability among a series of small molecule drugs).[50,51,56] As shown in Fig.4, the present study supports such an assessment (an R^2 value of 0.730 for P_{m}). This result may appear confusing given that (1) for four out of six small molecule drugs, the membrane only plays a very minor role (less than 1%) in resisting permeation, as compared to the UWL and (2) (de-)protonation plays

an important role as the permeant traverses the membrane. It is particularly puzzling that P^*_{m}, which in theory should be an improved version of P_{m} (by considering (de-)protonation), reflects a deteriorated correlation, with an R^2 value of 0.408.

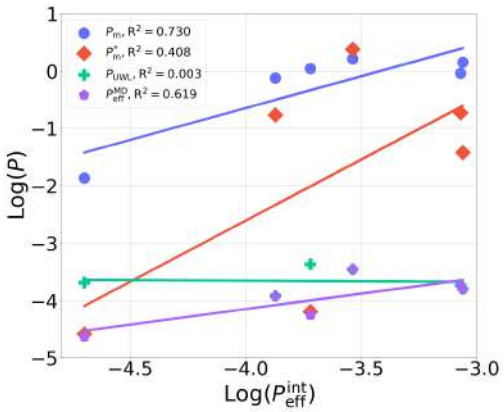

Figure 4: Correlation between various MD-based permeabilities ($\mathrm{P_m}$, $\mathrm{P^*_m}$, $\mathrm{P_{UWL}}$, $\mathrm{P^{MD}_{eff}}$) and the intestinal perfusion permeability ($\mathrm{P^{int}_{eff}}$).

It therefore remains unclear how the ISD model alone has any credibility for the prediction of the *relative* permeability; the observed good correlation may simply be a fluke. It is also noteworthy to point out that in spite of potentially being the rate-limiting step for many small molecule drugs, the UWL (and associated permeability, $\mathrm{P_{UWL}}$), can not distinguish the *relative* permeability for a chemically diverse series of permeants. Instead, since the permeability associated with the UWL is similar for all six small-molecule drugs studied here (Table 1), $\mathrm{P_{UWL}}$ contribution represents an upper limit of the permeability for both hydrophobic and hydrophilic molecules.

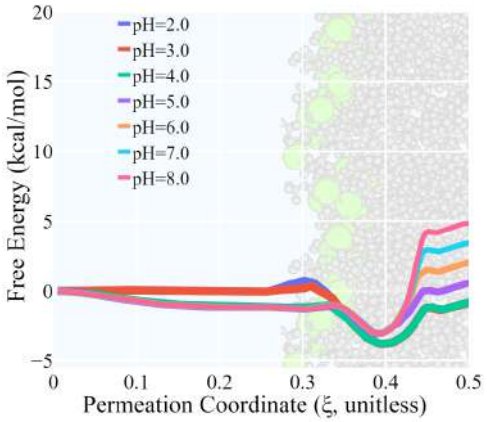

Figure 5: The hybrid MFEP of ketoprofen permeation when the aqueous solution pH is varied between 2.0 and 8.0.

As noted in the previous section, the free energy differences between the neutral and charged species in bulk water are determined from the difference between the pH and pK_a values (Eq. 6). The present work focuses on the permeation of small-molecule drugs at pH 7 (i.e., the average pH of intestinal fluid[43]) but this model can easily be extended to permeation in different regions of the gastrointestinal tract (e.g., stomach, pH 1.5-3.5; jejunum, pH 7-8; duodenum, pH 6), as the hybrid free energy surface of permeation at various pH can be created by adjusting the free energy differences between the neutral and charged species, following the same procedure as discussed above. Here, as an example, the permeation of ketoprofen (a weak acid, p$K_a = 4.0$) in a large pH range (2-8) is shown in Figure 5. This example clearly demonstrates that as the pH decreases, the free energy barrier against permeation decreases, indicating that for ketoprofen, absorption is limited by its diffusion through the UWL throughout the gastrointestinal tract. Allowing the permeant to change its protonation state also has potential ramifications far beyond small-molecule drug development. For example, amino acids in peptide-based drugs can also adopt different protonation states when interacting with the lipid bilayer, which could play an essential role in possible secondary-structure changes and impact membrane permeability. It is also important to note that the permeation hybrid free energy surface is constructed under the assumption

that the protonation state of the lipid head groups remains unaffected at different pH values. In principle, the protonation state of these head groups should also be determined according to the pH.

We have underscored in this work that the permeation of small molecule drugs primarily results from of at least two sources of resistance—traversing the membrane and diffusing through the UWL. Depending on the chemical properties of the permeant, one could completely overwhelm the other. Our investigation leads to the conclusion that if the molecule of interest has a permeation free energy that can be reasonably inferred, the study should only focus on the rate-limiting factor (either traversing the membrane or diffusing through the UWL). Conversely, should the permeation free energy of the molecule of interest be completely unknown, the study should start with characterizing the hybrid free energy of permeation that allows for (de-)protonation. It is also important to note that the exact calibration of the UWL thickness not only depends upon the nature of the permeant but also on its location in the gastrointestinal tract. For example, in the case of carbon dioxide and warfarin, Pohl et al.[53] assessed that the ratio $\delta_{\mathrm{UWL,CO_2}}/\delta_{\mathrm{UWL,warfarin}}$ could vary by up to 15%. Further studies are also necessary to expand this protocol to small-molecule drugs with multiple titatable sites such as methyldopa or amoxicillin.

Methods

$G(\xi)$, The free energy of permeation

The free energy of the permeation, $G(\xi)$, is computed with transition-tempered metadynamics[32] (TTMetaD). TTMetaD belongs to the family of metadynamics[57,58] (MetaD), in which sampling is facilitated by augmenting the Hamiltonian of the system with an additional bias potential that acts on a select number of degrees of freedom, often referred to as collective variables (CVs). These CVs are defined as a set of n functions acting on the microscopic

coordinates Q of the system at time t:

$$\overrightarrow{S}(Q(t)) = (s_1(Q(t)), s_2(Q(t)), ..., s_n(Q(t))) \in \mathbb{R}^n \tag{10}$$

At time t, the bias potential, V_G, on the CVs is then defined as:

$$V_G(\overrightarrow{S}(t), t) = \sum_{j<t/\tau} w \cdot \exp\left(-\sum_{i=1}^{n} \frac{(s_i(Q(j\tau)) - s_i(Q(t)))^2}{2\sigma_i^2}\right) \tag{11}$$

where τ is the gaussian deposition stride, w is the gaussian height, and σ_i is the gaussian width of the i^{th} CV. TTMetaD balances the exploration the CV space and the convergence of the bias energy by tracking the progress of the bias energy in filling the pre-defined free energy basins on the fly. Once a transition of the system between all pre-defined free energy basins is detected (e.g., an indicator of rough fulfillness of the underlying free energy surface), the gaussian height is aggressively tempered to facilitate convergence. In TTMetaD, the minimum bias on the maximally biased path connecting all pre-defined free energy basins, $V^*(t)$ is used to temper the height of the Gaussian hills as follows:

$$w(t) = w \cdot \exp\left(-\frac{\min[V^*(t)]}{k_B \Delta T}\right) \tag{12}$$

TTMetaD has proven to be an efficient method for computing the free energy of the permeation of small molecule drugs,[19,20,59]

Although a majority of previous in-silico studies utilize only one CV to describe the progress of the permeation (e.g., the center of mass (COM) distance between the drug and the lipid bilayer[18,24,30,60]), Sun et al. have shown that the orientation of the small molecule drug could have a significant impact on its interaction with the lipid bilayer. Therefore, two CVs (the COM distance between each of the two terminals of the small molecule and the lipid bilayer) are employed in this study - the mismatch between these two CVs indicates the orientation of the small molecule with respect to the membrane. The free energy of the

permeation, $G(\xi)$, is the minimum free energy path (MFEP) on the two-dimensional free energy surface calculated from the string method at zero Kelvin.[47] Last, convergence of the free energy calculations are shown in Figures S8 and S9 as the average standard deviation between replicas for all neutral and charged permeants, respectively.

Diffusivity of the permeant, $D(\xi)$

The diffusivity, $D(\xi)$, characterizes the speed of the diffusion of the small molecule drug along ξ. To calculate $D(\xi)$, a series of two-dimensional umbrella sampling simulations[61] are prepared, in each of which the small molecule drug is restrained to different points along ξ (corresponding to different values of CV1 and CV2). For each simulation, the time evolution of the system in the CV space, $\overrightarrow{S}(t)$ is orthogonally projected onto the MFEP. The arc length between this projected point and the origin of R is denoted as $l(t) \in \mathbb{R}$. $l(t)$ is collected from the simulation and $D(\xi)$ is computed as:[62]

$$D(\xi) = \frac{[\sigma^2(l)]^2}{\int_0^\infty C_l(t)dt} \tag{13}$$

$\sigma^2(l)$ and $C_l(t)$ are the variance and the autocorrelation function of $l(t)$, respectively. $C_l(t)$ is computed as:

$$C_l(t) = \frac{\Delta t}{t_s - t} \sum_{i=1}^{(t_s-t)/\Delta t} (l(i \cdot \Delta t) - \bar{l}) \cdot (l(i \cdot \Delta t + t) - \bar{l}) \tag{14}$$

in which t_s is the length of the umbrella sampling MD after initial equilibration, Δt is the MD integration time step, and $\bar{l}$ is the average of $l(t)$ over t_s.

The Hybrid Free Energy Surface of the Permeation

The protonation state of small molecules is highly dependent on their local chemical environment. In bulk water (pH 7), a drug-like small molecule is most likely to carry a net charge (see Table 1 for the pK_a values of the six small molecules in this study). Charged species

will incur a large free energy barrier permeating through the membrane. The high permeation barrier can be reduced if the molecule is neutralized *via* protonation/deprotonation at the surface of the lipid bilayer. It has been demonstrated that at the bilayer-water interface, the pK_{a} of small drug-like molecules reaches approximately 7.025,[63] as such, protonation/deprotonation should accompany the translocation of small molecules through lipid membranes. A standard approach[64] that has seen promising results is to compute the free energy of the permeation of small molecules at two different protonation states, and these two free energies are overlaid on top of one another, with the free energy difference of the small molecules in bulk water shifted according to their pK_{a} values (Eq. 6). The actual free energy of the permeation is determined as: 1) the lower of the two surfaces (e.g., starting from bulk water, the small molecule will be in a charged state) and 2) can transit to a different state when the two surfaces intersect to ensure 1). As such, the small molecule permeates through the membrane *via* a "path of least resistance", the MFEP found on the hybrid free energy surface.

Details of the Molecular Dynamics Simulations

The lipid bilayers in this research are set up using the CHARMM-GUI[65] membrane builder[66] and are composed of two leaflets of 16 POPC molecules each, centered in a rectangular box of approximately 3.3 x 3.3 x 13 nm. The bilayer is solvated by 3331 molecules of water and periodic boundary conditions are enforced in every direction. One small molecule drug (structures shown in Fig. 1) is solvated into each of the 6 systems. CHARMM36,[67] CHARMM general force fields (CGenFF),[31] and TIP3[68] forcefields are used to model the lipids, small molecule drugs, and water molecules, respectively. The initial structure of the bilayer is equilibrated with Gromacs-2020.4[13] patched with PLUMED2.4[69] (including TTMetaD[32] developed by the Voth research group) following regular MD convention. After the initial 5000 steps of steepest descent minimization, six stages of equilibration that systematically increase the time step and decrease the restraints on the lipid molecules is carried

out. The first two steps (NVT ensemble) of equilibration are carried out starting with a 1 fs time step, and the Berendsen weak coupling method[70] is used as the thermostat to maintain a temperature of 310.15 K with a time constant of 1 ps. The third stage (NPT ensemble) is performed using a 1 fs time step and the Berendsen weak coupling method to maintain pressure isotropically at 1.0 bar with a compressibility constant of 4.5×10^{-5} bar^{-1} . For the remaining three steps, the time step is increased to 2 fs and the restraints continually decrease to zero. A 100 ns AA MD simulation is then carried out to further equilibrate each system with an NPT ensemble maintained at 310.15 K and 1.0 bar using the Nose-Hoover thermostat[71] and the Parrinello-Rahman barostat,[72] respectively. The cut-off distance for the short-range nonbonded interactions is 1.2 nm, with electrostatic interactions calculated using the particle-mesh Ewald method.[73] Constraints are imposed on all the simulations using the LINCS algorithm.[74] The size of the system and details of MD simulations have been proven to give accurate results for studying the permeation of small molecules.

For every small molecule drug in their neutral and charged state, five independent 2+ microsecond replicas of TTMetaD simulations are carried out. These replicas start from the same initial configuration, but the velocities of the atoms are randomly generated from a Boltzmann distribution for each replica. The Gaussian bias energy deposition rate (τ in Eq. 11) is every 500 steps with a height of 0.015 kcal/mol (w) and a width of 0.22 nm (σ). The height of the Gaussian is tempered with a bias factor of 10 (i.e., ΔT in Eq. 4). The TTMetaD wells are located at (0.0, 0.0) and (0.48, 0.48) in the CV space. A bias threshold is 6.0 kJ/mol for the neutral species or 12 kJ/mol for the charged species. The bias threshold is added to delay the tempering of the height of the Guassian to ensure the exploration of TTMetaD. The two-dimensional free energy of the permeation is obtained from symmetrizing and averaging the inverse of the bias energy from each replica. After generating the hybrid surface as previously mentioned, $G(\xi)$ is calculated from the MFEP. The two-dimensional umbrella sampling is also carried out with the same system. The small molecule drug is first pulled to the desired position with the "MOVINGRESTRAINT" function in PLUMED, and

then restrained by a harmonic bias for a total of 200 ns. To ensure the system is fully relaxed, the autocorrelation function is collected from only the last 100 ns. The total simulation time for this research exceeds 130 microseconds.

Supporting Information Available

Additional information of the hybrid surfaces, visualizations of the permeants, individual 2D-PMFs, MFEPs and diffusion coefficient profiles can be found in the supporting information online (PDF).

Corresponding Author Information

Corresponding author e-mail: ruisun@hawaii.edu

Author Contributions

C.K., R.S. and C.C. reviewed and wrote the manuscript, C.K. and A.S. carried out the calculations, C.K. processed and analyzed the data.

Acknowledgement

The authors thanks the Information and Technology Services (ITS) from the University of Hawai'i, Manoa, XSEDE for the computational resources. and Eli Lilly and Company for the financial support.

Abbreviations Used

UWL, unstirred water layer; PMF, potential of mean force; MFEP, minimum free energy path; MetaD, metadynamics; TTMetaD; transition-tempered metadynamics; POPC, 1-palmitoyl-2-oleoyl-glycero-3-phosphocholine; ISD, inhomogeneous solubility diffusion; BCS, biopharmaceutics classification system; QSPR, quantitative structure–property relationship;

References

(1) Stamatis, S. D.; Rose, J. P. Lilly Absorption Modeling Platform: A Tool for Early Absorption Assessment. *Molecular Pharmaceutics* **2021**, *19*, 213–226.

(2) Maher, S.; Brayden, D. J. Overcoming poor permeability: translating permeation enhancers for oral peptide delivery. *Drug Discovery Today: Technologies* **2012**, *9*, e113–e119.

(3) Maher, S.; Brayden, D. J.; Casettari, L.; Illum, L. Application of permeation enhancers in oral delivery of macromolecules: an update. *Pharmaceutics* **2019**, *11*, 41.

(4) Maher, S.; Brayden, D. J. Formulation strategies to improve the efficacy of intestinal permeation enhancers. *Advanced Drug Delivery Reviews* **2021**, *177*, 113925.

(5) Dahlgren, D.; Roos, C.; Sjögren, E.; Lennernäs, H. Direct in vivo human intestinal permeability (Peff) determined with different clinical perfusion and intubation methods. *Journal of pharmaceutical sciences* **2015**, *104*, 2702–2726.

(6) Lennernäs, H. Intestinal permeability and its relevance for absorption and elimination. *Xenobiotica* **2007**, *37*, 1015–1051.

(7) Lee, J. B.; Zgair, A.; Taha, D. A.; Zang, X.; Kagan, L.; Kim, T. H.; Kim, M. G.; Yun, H.-y.; Fischer, P. M.; Gershkovich, P. Quantitative analysis of lab-to-lab variability in

Caco-2 permeability assays. *European Journal of Pharmaceutics and Biopharmaceutics* **2017**, *114*, 38–42.

(8) Volpe, D. A. Variability in Caco-2 and MDCK cell-based intestinal permeability assays. *Journal of pharmaceutical sciences* **2008**, *97*, 712–725.

(9) Roos, C.; Dahlgren, D.; Sjogren, E.; Tannergren, C.; Abrahamsson, B.; Lennernas, H. Regional intestinal permeability in rats: a comparison of methods. *Molecular pharmaceutics* **2017**, *14*, 4252–4261.

(10) Wang, Y.; Chen, X. QSPR model for Caco-2 cell permeability prediction using a combination of HQPSO and dual-RBF neural network. *RSC advances* **2020**, *10*, 42938–42952.

(11) Egan, W. J.; Lauri, G. Prediction of intestinal permeability. *Advanced drug delivery reviews* **2002**, *54*, 273–289.

(12) Adson, A.; Burton, P. S.; Raub, T. J.; Barsuhn, C. L.; Audus, K. L.; Ho, N. F. Passive diffusion of weak organic electrolytes across Caco-2 cell monolayers: Uncoupling the contributions of hydrodynamic, transcellular, and paracellular barriers. *Journal of pharmaceutical sciences* **1995**, *84*, 1197–1204.

(13) Abraham, M. J.; Murtola, T.; Schulz, R.; Páll, S.; Smith, J. C.; Hess, B.; Lindahl, E. GROMACS: High performance molecular simulations through multi-level parallelism from laptops to supercomputers. *SoftwareX* **2015**, *1*, 19–25.

(14) Gotz, A. W.; Williamson, M. J.; Xu, D.; Poole, D.; Le Grand, S.; Walker, R. C. Routine microsecond molecular dynamics simulations with AMBER on GPUs. 1. Generalized born. *Journal of chemical theory and computation* **2012**, *8*, 1542–1555.

(15) Salomon-Ferrer, R.; Gotz, A. W.; Poole, D.; Le Grand, S.; Walker, R. C. Routine microsecond molecular dynamics simulations with AMBER on GPUs. 2. Explicit solvent particle mesh Ewald. *Journal of chemical theory and computation* **2013**, *9*, 3878–3888.

(16) Simonson, T.; Archontis, G.; Karplus, M. Free energy simulations come of age: Protein-ligand recognition. *Accounts of chemical research* **2002**, *35*, 430–437.

(17) Chipot, C.; Comer, J. Subdiffusion in membrane permeation of small molecules. *Scientific Reports* **2016**, *6*, 35913.

(18) Tse, C. H.; Comer, J.; Sang Chu, S. K.; Wang, Y.; Chipot, C. Affordable membrane permeability calculations: permeation of short-chain alcohols through pure-lipid bilayers and a mammalian cell membrane. *Journal of Chemical Theory and Computation* **2019**, *15*, 2913–2924.

(19) Shoji, A.; Kang, C.; Fujioka, K.; Rose, J. P.; Sun, R. Assessing the Intestinal Permeability of Small Molecule Drugs via Diffusion Motion on a Multidimensional Free Energy Surface. *Journal of Chemical Theory and Computation* **2021**, *18*, 503–515.

(20) Sun, R.; Dama, J. F.; Tan, J. S.; Rose, J. P.; Voth, G. A. Transition-tempered metadynamics is a promising tool for studying the permeation of drug-like molecules through membranes. *Journal of chemical theory and computation* **2016**, *12*, 5157–5169.

(21) Ghysels, A.; Krämer, A.; Venable, R. M.; Teague Jr, W. E.; Lyman, E.; Gawrisch, K.; Pastor, R. W. Permeability of membranes in the liquid ordered and liquid disordered phases. *Nature communications* **2019**, *10*, 5616.

(22) Ghysels, A.; Roet, S.; Davoudi, S.; van Erp, T. S. Exact non-Markovian permeability from rare event simulations. *Physical Review Research* **2021**, *3*, 033068.

(23) Krämer, A.; Ghysels, A.; Wang, E.; Venable, R. M.; Klauda, J. B.; Brooks, B. R.; Pastor, R. W. Membrane permeability of small molecules from unbiased molecular dynamics simulations. *The Journal of Chemical Physics* **2020**, *153*.

(24) Marrink, S.-J.; Berendsen, H. J. Simulation of water transport through a lipid membrane. *The Journal of Physical Chemistry* **1994**, *98*, 4155–4168.

(25) Tse, C. H.; Comer, J.; Wang, Y.; Chipot, C. Link between membrane composition and permeability to drugs. *Journal of chemical theory and computation* **2018**, *14*, 2895–2909.

(26) Overton, C. E. *Über die osmotischen Eigenschaften der lebenden Pflanzen-und Tierzelle*; Fäsi & Beer, 1895.

(27) Kleinzeller, A. Ernest Overton's contribution to the cell membrane concept: a centennial appreciation. *Physiology* **1997**, *12*, 49–53.

(28) Diamond, J. M.; Katz, Y. Interpretation of nonelectrolyte partition coefficients between dimyristoyl lecithin and water. *The Journal of membrane biology* **1974**, *17*, 121–154.

(29) Comer, J.; Chipot, C.; González-Nilo, F. D. Calculating position-dependent diffusivity in biased molecular dynamics simulations. *Journal of chemical theory and computation* **2013**, *9*, 876–882.

(30) Venable, R. M.; Kramer, A.; Pastor, R. W. Molecular dynamics simulations of membrane permeability. *Chemical reviews* **2019**, *119*, 5954–5997.

(31) Vanommeslaeghe, K.; Hatcher, E.; Acharya, C.; Kundu, S.; Zhong, S.; Shim, J.; Darian, E.; Guvench, O.; Lopes, P.; Vorobyov, I. et al. CHARMM general force field: A force field for drug-like molecules compatible with the CHARMM all-atom additive biological force fields. *Journal of computational chemistry* **2010**, *31*, 671–690.

(32) Dama, J. F.; Rotskoff, G.; Parrinello, M.; Voth, G. A. Transition-tempered metadynamics: robust, convergent metadynamics via on-the-fly transition barrier estimation. *Journal of Chemical Theory and Computation* **2014**, *10*, 3626–3633.

(33) Ingólfsson, H. I.; Melo, M. N.; Van Eerden, F. J.; Arnarez, C.; Lopez, C. A.; Wassenaar, T. A.; Periole, X.; De Vries, A. H.; Tieleman, D. P.; Marrink, S. J. Lipid organi-

zation of the plasma membrane. *Journal of the american chemical society* **2014**, *136*, 14554–14559.

(34) Ingólfsson, H. I.; Carpenter, T. S.; Bhatia, H.; Bremer, P.-T.; Marrink, S. J.; Lightstone, F. C. Computational lipidomics of the neuronal plasma membrane. *Biophysical journal* **2017**, *113*, 2271–2280.

(35) Fagerholm, U.; Lennernäs, H. Experimental estimation of the effective unstirred water layer thickness in the human jejunum, and its importance in oral drug absorption. *European journal of pharmaceutical sciences* **1995**, *3*, 247–253.

(36) Wilson, F. A.; Sallee, V. L.; Dietschy, J. M. Unstirred water layers in intestine: rate determinant of fatty acid absorption from micellar solutions. *Science* **1971**, *174*, 1031–1033.

(37) Avdeef, A.; Artursson, P.; Neuhoff, S.; Lazorova, L.; Gråsjö, J.; Tavelin, S. Caco-2 permeability of weakly basic drugs predicted with the Double-Sink PAMPA pKaflux method. *European journal of pharmaceutical sciences* **2005**, *24*, 333–349.

(38) Anderson, B.; Levine, A. S.; Levitt, D. G.; Kneip, J.; Levitt, M. D. Physiological measurement of luminal stirring in perfused rat jejunum. *American Journal of Physiology-Gastrointestinal and Liver Physiology* **1988**, *254*, G843–G848.

(39) Levitt, M. D.; Furne, J.; Strocchi, A.; Anderson, B. W.; Levitt, D. G., et al. Physiological measurements of luminal stirring in the dog and human small bowel. *The Journal of clinical investigation* **1990**, *86*, 1540–1547.

(40) Levitt, M. D.; Furne, J. K.; Levitt, D. G. Shaking of the intact rat and intestinal angulation diminish the jejunal unstirred layer. *Gastroenterology* **1992**, *103*, 1460–1466.

(41) Chipot, C. Predictions from First-Principles of Membrane Permeability to Small

Molecules: How Useful Are They in Practice? *Journal of Chemical Information and Modeling* **2023**, *63*, 4533–4544.

(42) Avdeef, A. Physicochemical profiling (solubility, permeability and charge state). *Current topics in medicinal chemistry* **2001**, *1*, 277–351.

(43) Evans, D.; Pye, G.; Bramley, R.; Clark, A.; Dyson, T.; Hardcastle, J. Measurement of gastrointestinal pH profiles in normal ambulant human subjects. *Gut* **1988**, *29*, 1035–1041.

(44) Fallingborg, J. Intraluminal pH of the human gastrointestinal tract. *Danish medical bulletin* **1999**, *46*, 183–196.

(45) Yue, Z.; Li, C.; Voth, G. A.; Swanson, J. M. Dynamic protonation dramatically affects the membrane permeability of drug-like molecules. *Journal of the American Chemical Society* **2019**, *141*, 13421–13433.

(46) McQuarrie, D. A.; Simon, J. D. *Physical chemistry: a molecular approach*; University science books Sausalito, CA, 1997; Vol. 1.

(47) Weinan, E.; Ren, W.; Vanden-Eijnden, E. Simplified and improved string method for computing the minimum energy paths in barrier-crossing events. *Journal of Chemical Physics* **2007**, *126*, 164103.

(48) Bennett, W. D.; Tieleman, D. P. The Importance of Membrane Defects Lessons from Simulations. *Accounts of chemical research* **2014**, *47*, 2244–2251.

(49) Pinot, M.; Vanni, S.; Ambroggio, E.; Guet, D.; Goud, B.; Manneville, J.-B. Feedback between membrane tension, lipid shape and curvature in the formation of packing defects. *BioRxiv* **2018**, 389627.

(50) Bennion, B. J.; Be, N. A.; McNerney, M. W.; Lao, V.; Carlson, E. M.; Valdez, C. A.; Malfatti, M. A.; Enright, H. A.; Nguyen, T. H.; Lightstone, F. C. et al. Predicting a

drug's membrane permeability: A computational model validated with in vitro permeability assay data. *The journal of physical chemistry B* **2017**, *121*, 5228–5237.

(51) Orsi, M.; Sanderson, W. E.; Essex, J. W. Permeability of small molecules through a lipid bilayer: a multiscale simulation study. *The Journal of Physical Chemistry B* **2009**, *113*, 12019–12029.

(52) Boegh, M.; Nielsen, H. M. Mucus as a barrier to drug delivery–understanding and mimicking the barrier properties. *Basic & clinical pharmacology & toxicology* **2015**, *116*, 179–186.

(53) Pohl, P.; Saparov, S. M.; Antonenko, Y. N. The size of the unstirred layer as a function of the solute diffusion coefficient. *Biophysical Journal* **1998**, *75*, 1403–1409.

(54) Gutman, M.; Nachliel, E. The dynamic aspects of proton transfer processes. *Biochimica et Biophysica Acta (BBA)-Bioenergetics* **1990**, *1015*, 391–414.

(55) Avdeef, A.; Nielsen, P. E.; Tsinman, O. PAMPA—a drug absorption in vitro model: 11. Matching the in vivo unstirred water layer thickness by individual-well stirring in microtitre plates. *European journal of pharmaceutical sciences* **2004**, *22*, 365–374.

(56) Bemporad, D.; Essex, J. W.; Luttmann, C. Permeation of small molecules through a lipid bilayer: a computer simulation study. *The Journal of Physical Chemistry B* **2004**, *108*, 4875–4884.

(57) Laio, A.; Parrinello, M. Escaping free-energy minima. *Proceedings of the national academy of sciences* **2002**, *99*, 12562–12566.

(58) Laio, A.; Gervasio, F. L. Metadynamics: a method to simulate rare events and reconstruct the free energy in biophysics, chemistry and material science. *Reports on Progress in Physics* **2008**, *71*, 126601.

(59) Kang, C.; Sun, R. Molecular dynamics study of the interaction between the N-terminal of α-synuclein and a lipid bilayer mimicking synaptic vesicles. *The Journal of Physical Chemistry B* **2020**, *125*, 1036–1048.

(60) Berendsen, H. J.; Marrink, S.-J. Molecular dynamics of water transport through membranes: Water from solvent to solute. *Pure and applied chemistry* **1993**, *65*, 2513–2520.

(61) Torrie, G. M.; Valleau, J. P. Nonphysical sampling distributions in Monte Carlo free-energy estimation: Umbrella sampling. *Journal of Computational Physics* **1977**, *23*, 187–199.

(62) Hummer, G. Position-dependent diffusion coefficients and free energies from Bayesian analysis of equilibrium and replica molecular dynamics simulations. *New Journal of Physics* **2005**, *7*, 34.

(63) Hamilton, J. A. Fatty acid transport: difficult or easy? *Journal of lipid research* **1998**, *39*, 467–481.

(64) Ulander, J.; Haymet, A. Permeation across hydrated DPPC lipid bilayers: simulation of the titrable amphiphilic drug valproic acid. *Biophysical journal* **2003**, *85*, 3475–3484.

(65) Jo, S.; Kim, T.; Iyer, V. G.; Im, W. CHARMM-GUI: a web-based graphical user interface for CHARMM. *Journal of computational chemistry* **2008**, *29*, 1859–1865.

(66) Lee, J.; Patel, D. S.; Ståhle, J.; Park, S.-J.; Kern, N. R.; Kim, S.; Lee, J.; Cheng, X.; Valvano, M. A.; Holst, O. et al. CHARMM-GUI membrane builder for complex biological membrane simulations with glycolipids and lipoglycans. *Journal of chemical theory and computation* **2018**, *15*, 775–786.

(67) Best, R. B.; Zhu, X.; Shim, J.; Lopes, P. E.; Mittal, J.; Feig, M.; MacKerell Jr, A. D. Optimization of the additive CHARMM all-atom protein force field targeting improved

sampling of the backbone ϕ, ψ and side-chain $\chi 1$ and $\chi 2$ dihedral angles. *Journal of chemical theory and computation* **2012**, *8*, 3257–3273.

(68) Jorgensen, W. L.; Chandrasekhar, J.; Madura, J. D.; Impey, R. W.; Klein, M. L. Comparison of simple potential functions for simulating liquid water. *The Journal of chemical physics* **1983**, *79*, 926–935.

(69) Tribello, G. A.; Bonomi, M.; Branduardi, D.; Camilloni, C.; Bussi, G. PLUMED 2: New feathers for an old bird. *Computer physics communications* **2014**, *185*, 604–613.

(70) Berendsen, H. J.; Postma, J. v.; Van Gunsteren, W. F.; DiNola, A.; Haak, J. R. Molecular dynamics with coupling to an external bath. *The Journal of chemical physics* **1984**, *81*, 3684–3690.

(71) Nosé, S. A molecular dynamics method for simulations in the canonical ensemble. *Molecular physics* **1984**, *52*, 255–268.

(72) Parrinello, M.; Rahman, A. Polymorphic transitions in single crystals: A new molecular dynamics method. *Journal of Applied physics*

(73) Essmann, U.; Perera, L.; Berkowitz, M. L.; Darden, T.; Lee, H.; Pedersen, L. G. A smooth particle mesh Ewald method. *The Journal of chemical physics* **1995**, *103*, 8577–8593.

(74) Hess, B.; Bekker, H.; Berendsen, H. J.; Fraaije, J. G. LINCS: A linear constraint solver for molecular simulations. *Journal of computational chemistry* **1997**, *18*, 1463–1472.

TOC Graphic